An Improved Near- to Far-Zone Transformation for the Finite-Difference Time-Domain Method

Torleif Martin, *Student Member, IEEE*

Abstract— Near- to far-zone transformation for the finite-difference time-domain (FDTD) method can be performed by integration of the equivalent electric and magnetic currents originating from scattered electric and magnetic fields on a surface enclosing the object. Normally, when calculating the surface integrals, either the electric or magnetic fields are averaged since the electric and magnetic fields are spatially shifted in the FDTD grid. It is shown that this interpolation is unnecessary and also less accurate than if an integration is performed on two different surfaces. It is also shown that the accuracy of the far-zone transformation can be further improved if the phase is compensated with respect to a second-order dispersion corrected wavenumber. For validation, scattering results for an empty volume, a circular disk, and a sphere are compared with analytical solutions.

Index Terms— FDTD methods.

I. INTRODUCTION

NEAR- to far-zone transformation in conjunction with finite-difference time-domain (FDTD) has lately become more frequently used. Due to the fast development of computers and the ability to model complex metal or dielectric objects, FDTD has become a powerful tool for antenna and radar cross-section (RCS) calculations. To the author's knowledge, the first published papers on near- to far-zone transformation for FDTD appeared in the early eighties by Umashankar and Taflove [1], [2]. Since then a number of such calculations have been published (for example, see [3]–[8], [10], [11]). The near- to far-zone transformation is normally performed in the frequency domain, which requires that the scattered fields are transformed into the frequency domain either by a discrete Fourier transform (DFT) or a fast Fourier transform (FFT). Luebbers *et al.* [4] and Yee *et al.* [5] derived similar time-domain far-zone transformations, which is well suited for problems where time-domain results or a large number of frequencies are required. The FDTD near- to far-zone transformation technique has also been extended to objects over lossy dielectric half-planes [6], [7]. Recently, Ramahi presented a near- to far-zone transformation using the Kirchhoff's surface-integral representation [8].

In an analytical case, equivalent electric and magnetic currents multiplied with a Green's function can be integrated on a surface enclosing the object yielding the far-zone fields. The analytical surface-equivalence theorem requires that both the electric and magnetic surface currents lies on the same surface. When applying this to FDTD, which has spatially shifted E- and H-fields, the normal procedure is to spatially average the tangential H-fields (or the E-fields) from two adjacent planes, so that the averaged fields represents the values at the grid plane where the tangential E-fields (or the H-fields) are positioned. This procedure is commonly used but seldom discussed in detail and among the published work on the subject referenced in this paper, it is only explicitly mentioned in [4]–[6] and in [11]. In other published work, the details of integrating the surface currents are not treated although, in some cases, the derivations indicate that this approach is used. Ramahi has shown that by using the Kirchhoff's surface integral representation instead of the traditional vector potentials, the field interpolation can be avoided [8].

In this paper, an integral procedure is presented which is based on the integration of equivalent surface currents but where field interpolation is avoided. This resides from the fact that the numerical interpretation of the equivalence theorem for FDTD uses the tangential electric and magnetic fields on two spatially shifted surfaces in order to reproduce the fields in a closed source-free region [9]. It will be shown that if these surfaces are treated separately a more accurate transform can be achieved than if averaged fields on a single surface are used. This requires that a proper choice of phase function is made. The remaining errors due to numerical dispersion can also be further reduced by a correction of the wave number. The wave number appears in the Green's function and a second-order approximation of the numerical wave number is used instead of the nondispersive wave number.

II. NEAR- TO FAR-ZONE TRANSFORMATION

The usual derivation procedure for near-zone to far-zone transformations starts with the surface equivalence theorem from which the equivalent electric and magnetic currents can be extracted on a surface enclosing the scattering object (or antenna). The scattered field in the far zone can then be derived by integrating the equivalent currents multiplied (or convolved in the time domain) with a free-space Green's function. Following the notation in [12], if the observation point is in the far field ($kr \gg 1$), the vector potentials $\boldsymbol{A}$ and $\boldsymbol{F}$ can be written as

$$\boldsymbol{A}(\boldsymbol{r}) = \frac{\mu\, e^{-jkr}}{4\pi r} \iint\limits_{S} \boldsymbol{J}_s\, e^{jk\hat{\boldsymbol{r}}\cdot\boldsymbol{r}'}\, dS' \tag{1}$$

$$\boldsymbol{F}(\boldsymbol{r}) = \frac{\varepsilon\, e^{-jkr}}{4\pi r} \iint\limits_{S} \boldsymbol{M}_s e^{jk\hat{\boldsymbol{r}}\cdot\boldsymbol{r}'}\, dS' \tag{2}$$

where the equivalent electric and magnetic surface currents are

$$\boldsymbol{J}_s = \hat{\boldsymbol{n}} \times \boldsymbol{H}$$
$$\boldsymbol{M}_s = -\hat{\boldsymbol{n}} \times \boldsymbol{E} \tag{3}$$

where the scattered electric and magnetic fields are assumed to be calculated on the same surface S. When applying this technique in FDTD calculations the above formula must be applied on the electric and magnetic fields extracted from the Yee grid. If the integration surface lies in the plane of tangential E-fields, the tangential H-fields values on the integration surface are usually obtained by interpolation of points on either side of the surface since the electric and magnetic fields are spatially shifted.

The electric field in the far zone can then be determined by [12]

$$E_\theta = -j\omega(A_\theta + \eta F_\phi) \tag{4}$$
$$E_\phi = -j\omega(A_\phi - \eta F_\theta) \tag{5}$$

where η is the free-space wave impedance. The spatially averaged fields will cause some errors in the transform that are negligible at low frequencies but, as the frequency increases, the phase shift between two cells in the Yee grid will be sufficiently high to introduce small but nonnegligible errors (mainly in phase) when interpolating the fields. When interpolating fields at different positions in the frequency domain, it would probably be preferable to use a geometric mean value instead of an arithmetic mean value, which has been demonstrated for impedance calculations in FDTD [13]. The reason for that is that a geometric mean value usually gives a better phase estimate between the two field components. However, below, it will be shown that the interpolation procedure is unnecessary and also slightly less accurate than if the integration is performed on two different surfaces.

The procedure above assumed that the only existing currents were surface currents on a *single* surface enclosing the object. One of the early published work where the equivalence theorem was utilized in conjunction with FDTD is the paper describing the Huygen's source implementation in FDTD [9]. The sources derived in [9] are placed on two different surfaces, one for the electric currents and one for the magnetic currents. In a rectangular FDTD grid, these currents flow at the surface of two different rectangular boxes separated a half-cell size.

In the case of Huygen's sources for reproducing the field inside the boxes with a zero field on the outside, assume that the outer box is defined by locations of tangential H-fields and the inner box is defined by the locations of tangential E-fields. In the FDTD advance equations, when updating the E-fields on the inner surface, the electric current J_s is added to the field-advance equations such as (6). Although J_s depends on the H-fields on the outer surface it should be regarded to be spatially located on the inner surface since it is a source for the electric fields. *Vice versa*, the magnetic currents are regarded to be spatially located on the outer surface although they depend on the electric field values on the inner surface. As an example, the field advance equations for $E_x(i, j, k)$ on
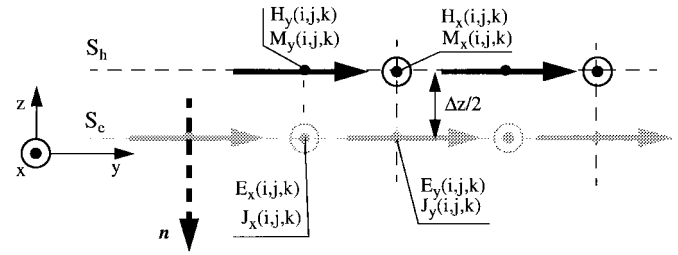

Fig. 1. FDTD grid at the boundary of the equivalent surfaces showing only the tangential components. The current component $J_x(i, j, k)$ is positioned at the same position as $E_x(i, j, k)$ and calculated using $H_y(i, j, k)$. The E_x and H_y fields lies $\Delta x/2$ above the E_y- and H_x fields (closer to the viewer).

an upper Huygen's XY surface are (see Fig. 1)

$$E_x^{n+1}(i, j, k) = E_x^n(i, j, k) + \frac{\Delta t}{\varepsilon \Delta y}$$
$$\cdot [H_z^{n+1/2}(i, j, k) - H_z^{n+1/2}(i, j-1, k)]$$
$$- \frac{\Delta t}{\varepsilon \Delta z}$$
$$\cdot [H_y^{n+1/2}(i, j, k) - H_y^{n+1/2}(i, j, k-1)]$$
$$- \frac{\Delta t}{\varepsilon \Delta z} J_x^{n+1/2}(i, j, k) \tag{6}$$

where

$$J_x^{n+1/2}(i, j, k) = H_y^{\text{inc}}[t = (n+1/2)\Delta t, i, j, k] \tag{7}$$

which will compensate for $H_y^{\text{inc}} = 0$ on the outer box ($\hat{\boldsymbol{n}} = -\hat{z}$ in this case). Note that the source appears at the position of the E_x field but depends on a H_y field a half cell from the E_x field in the direction perpendicular to the surface. The surface current is actually converted into an equivalent volume current since it is divided with the thickness of the layer (Δz) in (6).

Generally, denoting the outer surface S_h and the inner surface S_e, the equivalent currents that reproduce the fields inside a closed volume can be written as

$$\boldsymbol{J}_s|_{S_e} = \hat{\boldsymbol{n}} \times \boldsymbol{H}|_{S_h} \tag{8}$$
$$\boldsymbol{M}_s|_{S_h} = -\hat{\boldsymbol{n}} \times \boldsymbol{E}|_{S_e} \tag{9}$$

where $\hat{\boldsymbol{n}}$ is the surface normal pointing into the volume and $\boldsymbol{E}$ and $\boldsymbol{H}$ are the fields that will be reproduced inside the volume.

The coordinates of the field values on the right-hand side (RHS) of (8) and (9), relative to the current positions, are shifted a half-cell size in the direction parallel to the surface normal (see Fig. 1). In the context of a Huygen's source in FDTD, these currents fully reproduce the fields inside the volume; that is, if dispersion errors are ignored.

By changing the direction of the surface normal these currents will reproduce the fields outside a volume due to the sources inside it, as in the case of the near-zone to far-zone transformation. Inserting (8) and (9) in (1) and (2), denoting the source vector spanning the S_e surface by $\boldsymbol{r}'_e$ and the source vector spanning the S_h surface by $\boldsymbol{r}'_h$ yields

$$\boldsymbol{A}(\hat{\boldsymbol{r}})_{\text{FDTD}} = \frac{\mu e^{-jkr}}{4\pi r} \iint_{S_e} \hat{\boldsymbol{n}} \times \boldsymbol{H}|_{S_h} e^{jk\hat{\boldsymbol{r}}\cdot\boldsymbol{r}'_e} \, dS' \tag{10}$$

$$\boldsymbol{F}(\hat{\boldsymbol{r}})_{\text{FDTD}} = -\frac{\varepsilon e^{-jkr}}{4\pi r} \iint_{S_h} \hat{\boldsymbol{n}} \times \boldsymbol{E}|_{S_e} e^{jk\hat{\boldsymbol{r}}\cdot\boldsymbol{r}'_h} \, dS'. \tag{11}$$

Note that the integrals in (10) and (11) depend on phase factors calculated at a different position than the position of the fields. The integration is performed on two different surfaces using the source fields at the "dual" surface. In the following text this integration procedure will, therefore, be regarded as a *mixed surface* transform, while using a single surface in combination with averaged fields will be called *single surface* transform. By replacing the integrals by sums this can be easily incorporated in the FDTD code. It can be shown that the mixed-surface transform is consistent with respect to the numerical equivalence of the reciprocity theorem if the equivalent sources are created using the method in [9]. By using the mixed surface transform instead of using averaged field values at a single surface, a large number of numerical interpolation operations can be saved. It will also be shown to be more accurate than the interpolation procedure. The concepts can also be applied in the time-domain far-zone transformation. In this case, the retarded times that determines the time samples of the field to be used must be calculated using the position of the current vector at the "dual" surface. The corresponding expressions for the vector potentials in the time domain at a distance r are

$$A(\boldsymbol{r}, t)_{\mathrm{FDTD}} = \frac{\mu}{4\pi r}$$
$$\iint\limits_{S_e} \hat{\boldsymbol{n}} \times \boldsymbol{H}|_{S_h} \left[t - \left(\frac{r - \hat{\boldsymbol{r}} \cdot \boldsymbol{r}'_e}{c} \right) \right] dS' \tag{12}$$

$$F(\boldsymbol{r}, t)_{\mathrm{FDTD}} = -\frac{\varepsilon}{4\pi r}$$
$$\iint\limits_{S_h} \hat{\boldsymbol{n}} \times \boldsymbol{E}|_{S_e} \left[t - \left(\frac{r - \hat{\boldsymbol{r}} \cdot \boldsymbol{r}'_h}{c} \right) \right] dS'. \tag{13}$$

Note that the H-fields in (12) are extracted at a time step determined by the retarded time calculated at the surface of tangential E-fields. The opposite holds for the E-fields in (13). When extracting the fields linear interpolation between two time steps should be used if the time delay is a decimal fraction, as described in [4]. The scattered E-field in the far zone can then be calculated by the corresponding time-domain expressions for (4) and (5) (replacing $j\omega$ with a time derivative).

III. VERIFICATION IN FREE-SPACE

Normally, when using Huygen's sources for creating a plane wave in scattering problems, the equivalent currents used for far-zone transformation are determined on a closed surface outside the Huygen's sources so that only the scattered fields are transformed. One way of examining the properties of the far-zone transformation routine is to apply it on a plane wave propagating through the computational volume with no scattering object present, simply by placing the transformation surface *inside* the Huygen's sources. Considering the analytical case, since the plane wave is source-free within the surface where the far-zone transformation is applied, the transformation will result in zero scattered fields in all
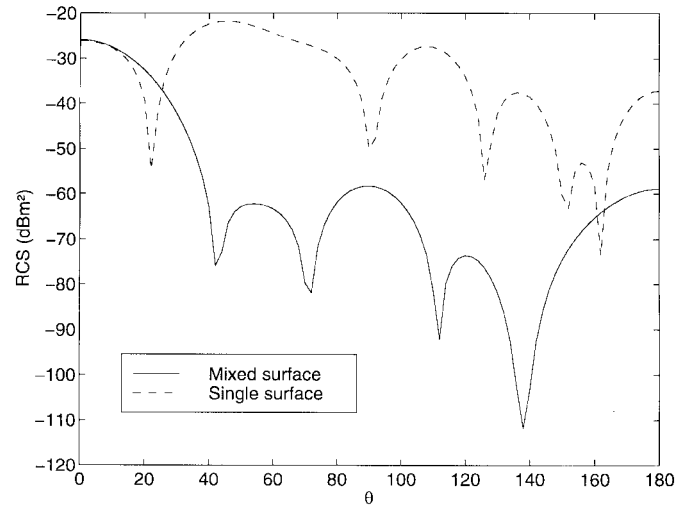

Fig. 2. Numerical bistatic RCS of an empty FDTD volume $20 \times 20 \times 20$ cells. The frequency is 2 GHz, which corresponds to $\lambda = 15\Delta x$. The plane wave is incident from $180°$.

directions. However, in the numerical case the FDTD suffers from dispersion, which will cause distortions depending on the propagated path length of the plane wave. The distortion will then vary along the sides of the surface where the equivalent currents are determined. This will lead to an erroneous field that does not cancel in all directions.

To illustrate the different transform methods a plane wave was created using a surface of Huygen's sources spanning a volume of $30 \times 30 \times 30$ cells. The Gaussian pulsed plane wave was propagating in the positive z direction. Inside the Huygen's sources the far-zone integration procedure was applied on a surface enclosing a volume by $20 \times 20 \times 20$ cells. The equivalent currents on this surface were transformed into the frequency domain by a DFT while marching in time. The scattered field expressed as a bistatic radar cross section at 2 GHz as function of the polar angle θ is shown below (the plane wave was incident from $180°$). The cell size was 0.01 m in all directions.

As seen from Fig. 2, the RCS of both transformations has a common local maximum in the forward direction ($0°$) which is expected since the distorted plane wave is propagating in this direction and the far-zone contribution of the two opposite surfaces of the computational volume are subtracted slightly out of phase. In this case, the phase error is proportional to the propagated path length in the computational volume. For the single-surface transformation the highest maximum occurs at about $45°$. Using the mixed surface concepts reduces the error dramatically at all other angles. The maximum value at $0°$ is about -26 dBm^2 (which corresponds the area of 25 FDTD grid cells). This can be compared with the maximum RCS of a perfectly conducting target in FDTD consisting of only one single E-field component, which is approximately -56 dBm^2 at this frequency ($\Delta x = 0.01$ m).

At other angles the errors using the mixed-surface transform are significantly lower than the errors produced using a single-surface transform. The error can be even further reduced if the dispersion relationship is taking into account when transforming the fields to the far zone.

IV. DISPERSION COMPENSATION

The near- to far-zone transformation can be improved even further if performed in the frequency domain. By adjusting the phase factor $e^{(jk\hat{r}\cdot r')}$ in (10) and (11) to the true numerical phase factor valid in the FDTD grid, the far-zone transformation errors due to dispersion can be further reduced. The dispersion relationship for the FDTD-grid can be derived as [14]

$$\left[\frac{1}{c\Delta t}\sin\left(\frac{\omega\Delta t}{2}\right)\right]^2 = \left[\frac{1}{\Delta x}\sin\left(\frac{\tilde{k}_x\Delta x}{2}\right)\right]^2$$
$$+ \left[\frac{1}{\Delta y}\sin\left(\frac{\tilde{k}_y\Delta y}{2}\right)\right]^2 + \left[\frac{1}{\Delta z}\sin\left(\frac{\tilde{k}_z\Delta z}{2}\right)\right]^2 \quad (14)$$

where $\tilde{k}$ is the numerical wavevector. Thus, using $\tilde{k}$ instead of $k\hat{r}$ in the exponent of the phase factor, a reduction of the error can be expected. This is difficult, however, since solving (14) for $\tilde{k}_x$, $\tilde{k}_y$, and $\tilde{k}_z$ are not straightforward. An approximate solution can be found by using series expansions for $\sin x$. The technique has been used when analyzing nonuniform grids in [15], although a slightly different approach is used in the derivation below. Expressing $\tilde{k}$ as

$$\tilde{k} = \tilde{k}\hat{r} = \tilde{k}(s_x\hat{x} + s_y\hat{y} + s_z\hat{z}) \quad (15)$$

where

$$s_x = \cos\varphi\sin\theta$$
$$s_y = \sin\varphi\sin\theta$$
$$s_z = \cos\theta \quad (16)$$

and expanding the $\sin^2(x)$ terms on the RHS of (14) and retaining second-order terms yields

$$\left[\frac{1}{c\Delta t}\sin\left(\frac{\omega\Delta t}{2}\right)\right]^2 \approx \frac{\tilde{k}^2}{2} - \frac{\tilde{k}^4}{48}(s_x^4\Delta x^2 + s_y^4\Delta y^2 + s_z^4\Delta z^2). \quad (17)$$

The solution to this equation is given by

$$\tilde{k} = \sqrt{\frac{6}{p^2}\left\{1 - \sqrt{1 - \frac{4}{3}p^2\left[\frac{1}{c\Delta t}\sin\left(\frac{\omega\Delta t}{2}\right)\right]^2}\right\}} \quad (18)$$

where $p^2 = s_x^4\Delta x^2 + s_y^4\Delta y^2 + s_z^4\Delta z^2$. The highest level of dispersion occurs at propagation angles that are parallel to one of the Cartesian axes in the FDTD grid. In this case, a solution to (14) can easily be found. Consider for example that $\hat{r} = \hat{x}$ in (15). Equation (14) can then be rewritten as

$$\tilde{k} = \frac{2}{\Delta x}\arcsin\left[\frac{\Delta x}{c\Delta t}\sin\left(\frac{\omega\Delta t}{2}\right)\right]. \quad (19)$$
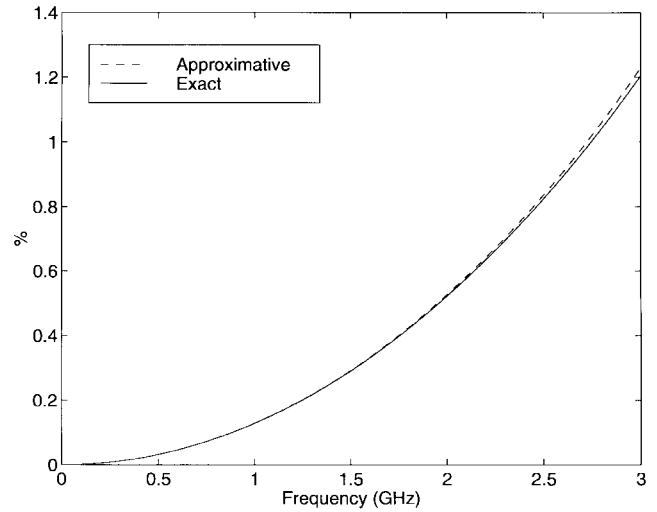

Fig. 3. Relative difference between numerical wavenumbers and analytical wavenumber for a plane wave propagating in the x direction. The curves are computed for a timestep of 95% of the three-dimensional Courant stability criterion.
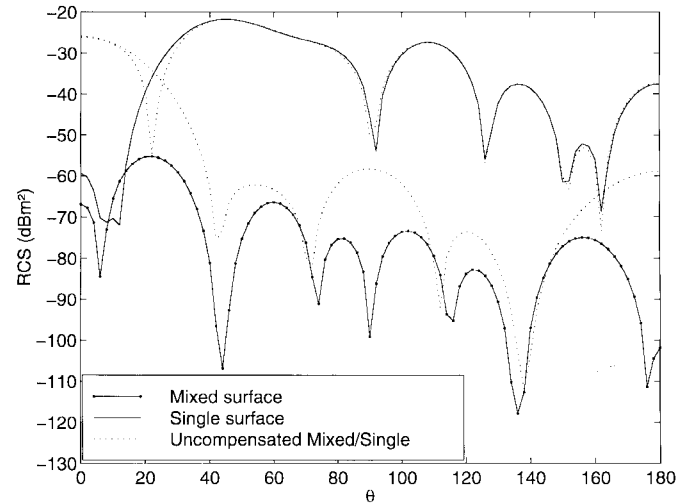

Fig. 4. Numerical bistatic RCS of an empty FDTD volume, $20 \times 20 \times 20$ cells. In both far-zone transforms a dispersion compensated wavenumber has been used. The frequency is 2 GHz, which corresponds to $\lambda = 15\Delta x$. The plane wave is incident from 180°. The uncompensated results according to Fig. 2 are also included as dotted lines.

To illustrate the accuracy of (18), the relative difference $(\tilde{k} - k)/k$, between $\tilde{k}$ as obtained from (18) and (19) and $k = \omega/c$, is shown in Fig. 3. The cell size is $\Delta x = 0.01$ m so that 3 GHz corresponds to a free-space wavelength of $10\Delta x$. As seen from the figure the correspondence is very good.

By using the compensated wavenumber from (18) in the phase factor when calculating the far-zone transformation the errors shown in Fig. 2 can be reduced. This is shown in Fig. 4. The level at 0° is dramatically reduced. At other angles the error is reduced several decibels for the mixed-surface transform. The single-surface transform is not affected at other angles than around 0°. The RCS of the empty volume when using the mixed-surface transform is below -55 dBm^2 for all angles, which corresponds to an area of 0.03 FDTD grid cells and which is approximately the maximum RCS of a single E-field, which is set to zero. Since the analytic solution (19) can be used instead of (18) at certain angles a
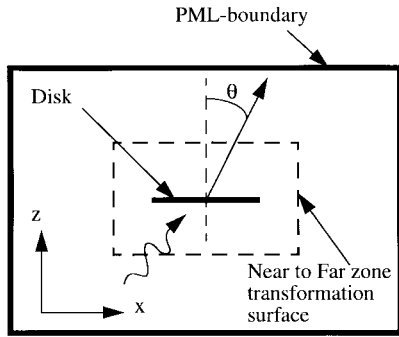
Fig. 5. Schematic drawing (XZ slice) of the computational volume.

far-zone computation was done at 0 and 180° using (19) in order to get an indication of where a possible lowest level of the compensated mixed-surface transform lies. At 0° the level was -88.5 dBm^2 and at 180° the level was -118 dBm^2. This is approximately 15–20 dBm^2 lower than the values at the corresponding scattering angles in Fig. 4. This type of compensation procedure is unfortunately difficult to implement in the time-domain version of the near- to far-zone transformation.

V. Scattering From Circular Disk

In order to verify a numerical model it is feasible to compare the numerical results with analytical results. A common used object for three-dimensional problems is the sphere of which an analytical solution exist (Mie series solution). Another object of which an analytical solution exists is the circular disk. This solution is also a series solution, although slightly more complex than the sphere solution. The solution used in this paper is based on expansion of the scattered field in spherical vector wavefunctions and the T-matrix method, published by Kristensson and Waterman [16].

A disk of radius 0.2 m was modeled in FDTD using a cell size of 0.01 m, which corresponds to 20 cells in radius. The computational volume was $120 \times 120 \times 80$ cells. The computations were performed using the scattered field formulation of FDTD. The integration surface for far-zone transformation was placed five cells from the disk at closest (35 cells from the outer boundary). In addition, a computation with a highly resolved disk (80 cells in radius) was done in one case for comparison in scattering regions with relatively large errors. The boundary condition was a six-layer perfectly matched layer (PML) [17] (a larger number of PML's were tested without any improvement of the results). A slice of the computational volume can be seen in Fig. 5.

The following examples will be discussed (see Fig. 5 for explanation of symbols).

1) Incident plane wave from $\theta = 240°$. Polarization perpendicular to plane of incidence (TE pol). Plane of incidence and scattering plane was in the XZ plane.
2) Plane of incident as in case 1, polarization parallel with the plane of incidence (TM pol). Scattering plane the same as the plane of incidence.
3) Plane of incident and polarization as in case 1 (TE pol), $\theta = 225°$, and scattering plane perpendicular to the plane of incidence (YZ plane).

In case numbers 1 and 2, the results are presented for θ values between 0 and 360°. In case number 3, the results are presented for θ-values between 0 and 90°. In computing number 3, both polarizations of the scattered field are created. The far-zone transformation was performed in the frequency domain in all cases.

When comparing the results with the analytical solution one must keep in mind that the spatial discretization in FDTD implies that the object is slightly larger than indicated by the coordinates of the tangential E-fields. This is due to the FDTD representation of the object by tangential E-fields that actually represents an average value over one cell. In accordance to the results presented by Trueman *et al.* [18], an adjustment of a half-cell of the disk radius was made when computing the analytical results, i.e., the radius was 0.205 m.

In order to facilitate the comparison, the results are presented in two diagrams covering 180° each of the 360° turn of θ. In order to demonstrate the improvements achieved by using both the mixed-surface transform and the dispersion correction, these results are compared with the single surface transform with no dispersion correction.

### A. Incident Plane Wave From $\theta = 240°$ TE-Polarization Scattering Plane = Incidence Plane

The bistatic RCS in the incident plane at 1.5 GHz is shown in Fig. 6. In this scattering plane only TE components contribute to the RCS. The magnitude correspondence with the analytical solution is improved when using the mixed-surface concept. The left peak at about 60° is due to the forward scattering and the right peak is the specular reflection. In the backscattering region the amplitudes are much lower than in the forward-scattering region. The correspondence between theory and calculations is, therefore, reduced and the difference is about 2 dB at most for the 20-cell-radius disk. The largest differences occur at scattering angles 90 and 270°, which corresponds to directions in the plane of the disk. In the backscattering region (180–360°) the results for the 80-cell-radius disk are also included. The resolution in this case corresponds to 80 cells per wavelength. As seen from Fig. 6(b), both transforms yield more accurate results as expected in this case, but the single-surface transform deviates more around 230 and 310°.

In Fig. 7 the results at 2 GHz are displayed. In the backscattering region (180–360°), the results for the 80-cell-radius disk are also included. The resolution in this case corresponds to 60 cells per wavelength. As seen from the diagrams the single-surface transformation results starts to deviate more from the analytical solution than the mixed-surface transformation results. Even at 60 cells per wavelength the error is over 2 dB for the single-surface transform but only 0.6 dB for the mixed-surface transform. In order to quantify the differences in error between the two methods, the linear relative error defined by
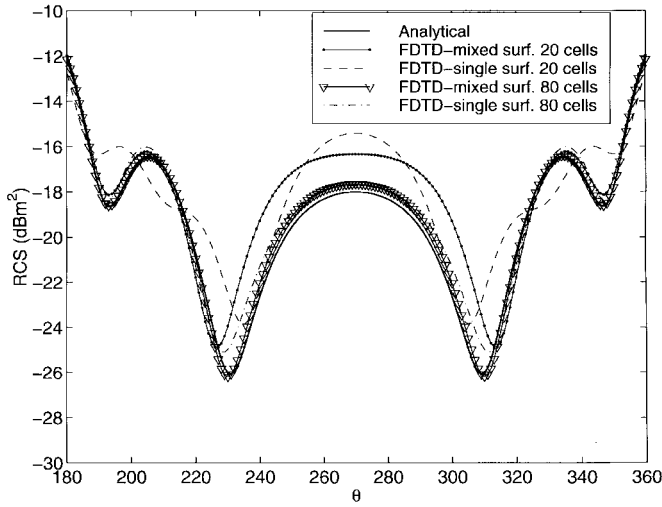
$$\eta_{\text{err}} = \frac{\sigma_{\text{FDTD}} - \sigma_{\text{Analytic}}}{\sigma_{\text{Analytic}}} \qquad (20)$$
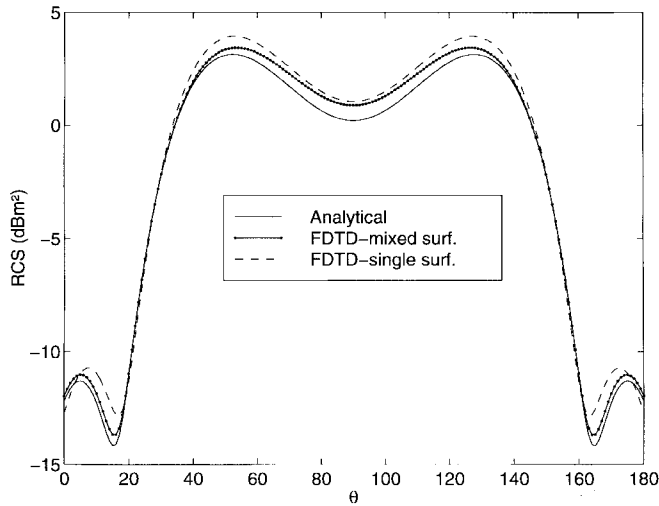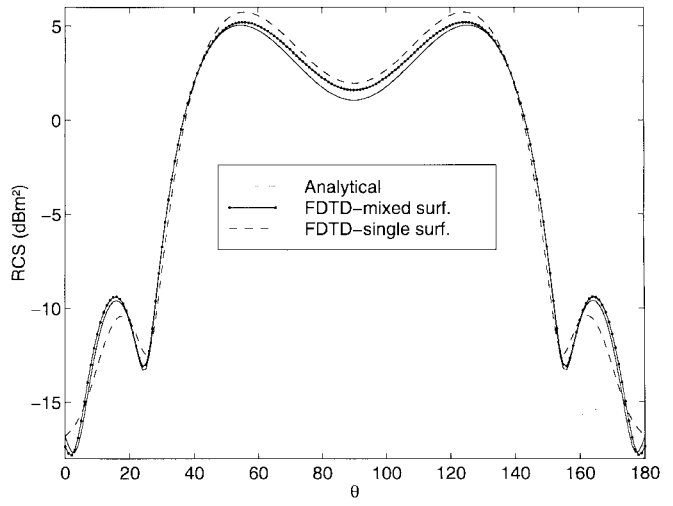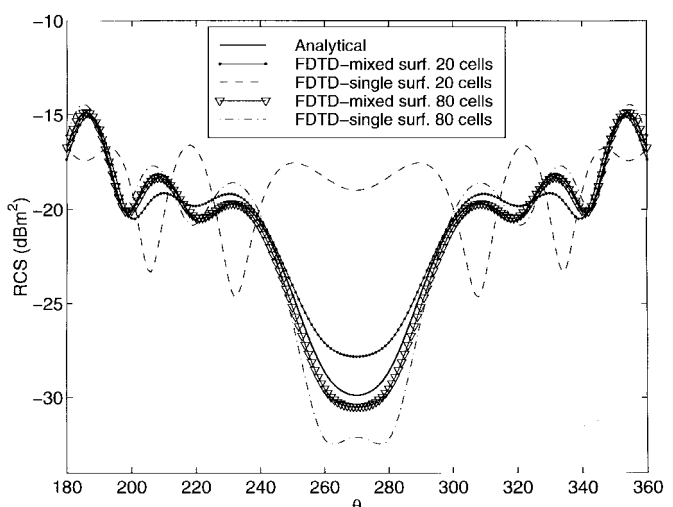
Fig. 6.   (a) Bistatic RCS of circular disk at 1.5 GHz ($\lambda = 20$ cells); TE pol.
Plane wave incidence from $\theta = 240°$. Scattering angle 0–180°. (b) Bistatic
RCS of circular disk at 1.5 GHz ($\lambda = 20$ cells and $\lambda = 80$ cells); TE pol.
Plane wave incidence from $\theta = 240°$. Scattering angle 180–360°.

Fig. 7.   (a) Bistatic RCS of circular disk at 2.0 GHz ($\lambda = 15$ cells); TE pol.
Plane wave incidence from $\theta = 240°$. Scattering angle 0–180°. (b) Bistatic
RCS of circular disk at 2.0 GHz ($\lambda = 15$ cells and $\lambda = 60$ cells); TE pol.
Plane wave incidence from $\theta = 240°$. Scattering angle 180–360°.

and the absolute error defined by

$$\sigma_{err} = \sigma_{FDTD} - \sigma_{Analytic} \tag{21}$$

was computed at 2 GHz between 0 and 360° for the different transformation methods. Additionally, to illustrate the influence of the dispersion compensation for both transforms, the results with and without the dispersion compensation was computed. The results for the 20-cell-radius disk are displayed in Figs. 8 and 9. In the forward-scattering region (between 0 and 180°) where the scattering amplitude is relatively high, the relative error is well below 20% for the mixed-surface transform. For the single-surface transform the errors are much higher. In this region, the dispersion compensation has a small but nonnegligible effect on the results. For the mixed-surface transform at most the relative error is reduced from 21.5 to 13% at 90°. In the backscattering region (between 180 and 360°), the relative errors are much higher due to the low amplitudes in this region. As seen from Figs. 8 and 9 the

mixed surface transform is much better also in this region. The dispersion compensation effects are negligible at these scattering angles. On an average, the mixed-surface transform reduces the error at least by a factor of two compared with the single-surface transform.

B. Incident Plane Wave from $\theta = 240°$, TM-Polarization Scattering Plane = Incidence Plane

When the polarization of the incident field lies in the plane of incidence (TM) the accuracy between the analytical solution and the numerical results is high for both the single-surface and the mixed-surface transform methods. The results at 2 GHz are displayed in Fig. 10(a) and (b). Between 0 and 180° the mixed-surface transform agrees excellent with the analytical solution, while the single-surface transform deviates slightly from the analytical solution. The agreement between the single-surface transform and the analytical solution between 180 and 360° is
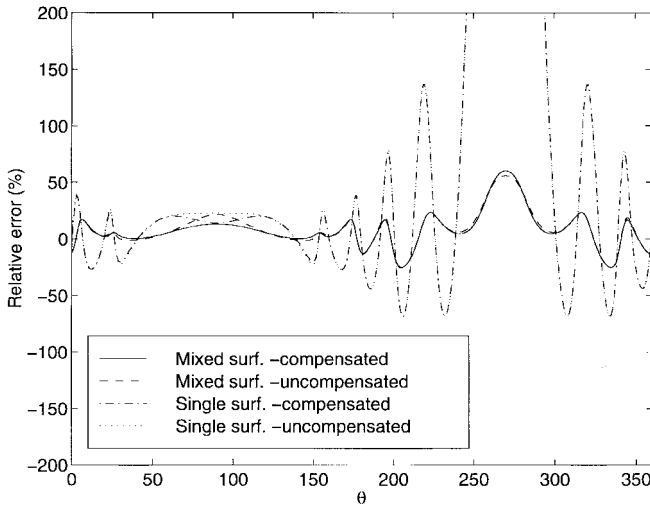
Fig. 8. Relative error of bistatic RCS between 0 and 360° at 2 GHz. The errors for the single-surface transform around 270° is not shown and exceeds 1000%.
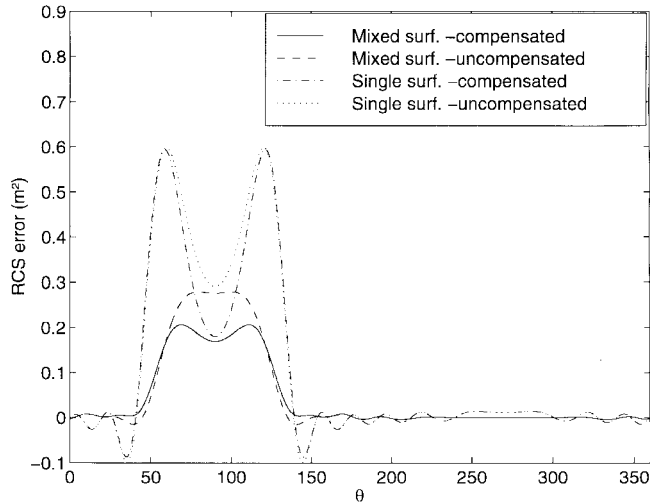

Fig. 9. Absolute error of bistatic RCS between 0 and 360° at 2 GHz.

(a)

(b)

Fig. 10. (a) Bistatic RCS of circular disk at 2.0 GHz ($\lambda = 15$ cells); TM pol. Plane wave is incident from $\theta = 240°$. Scattering angle 0–180°. (b) Bistatic RCS of circular disk at 2.0 GHz ($\lambda = 15$ cells); TM pol. Plane wave is incident from $\theta = 240°$. Scattering angle 180–360°.

much better in this case compared with the TE case. Close to the scattering angle 270° the single-surface transform agrees even better with the analytical solution than the mixed-surface transform. However, due to the low scattering amplitudes the uncertainty of the results is higher for both methods in this backscattering region compared with the forward-scattering region.

C. Incident Plane Wave from $\theta = 240°$ TE-Polarization Scattering Plane Perpendicular to Incidence Plane

In the third example, the scattering plane is perpendicular to the plane of incidence. In this plane, both polarizations of the scattered field will be created. The bistatic RCS at 2.5 GHz is displayed for the two polarizations separately in Figs. 11 and 12. The agreement is relatively good between both transform methods and the analytical solution despite the low-scattering amplitudes at these scattering angles. Generally, the mixed-surface transform agrees better with the analytical solution than the single-surface transform.
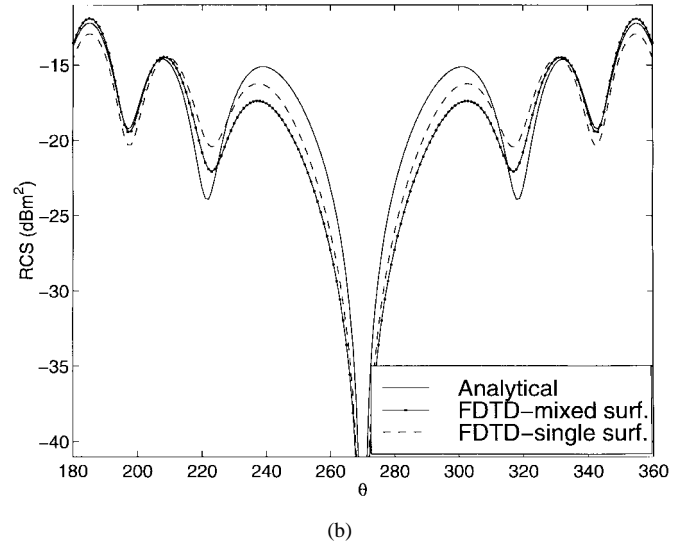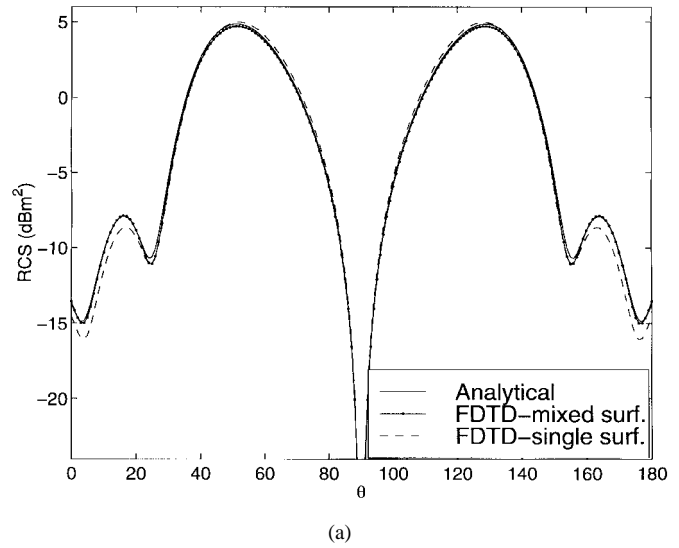
VI. MONOSTATIC SCATTERING FROM A SPHERE

An often used object in validation studies is the sphere since the analytical solution is widely known and examples can be found in most textbooks treating electromagnetic scattering problems. In this paper, we restrict ourselves to backscattering from a perfectly conducting sphere of radius 0.205 m, which was modeled in FDTD with a radius of 20 cells and a resolution of 0.01 m. The results for the monostatic RCS in a linear scale can be seen in Fig. 13, where the RCS has been normalized with the projected area of the sphere (πa^2). Since modeling the sphere with FDTD is a difficult problem due to the staircasing representation of the surface, it is difficult to compare the two transforms with the analytical solution at high frequencies. The presentation of the results are, therefore, limited to frequencies below 1 GHz, which corresponds to a wavelength >30 cells. Also, in this case, it is clear that the mixed-surface transform
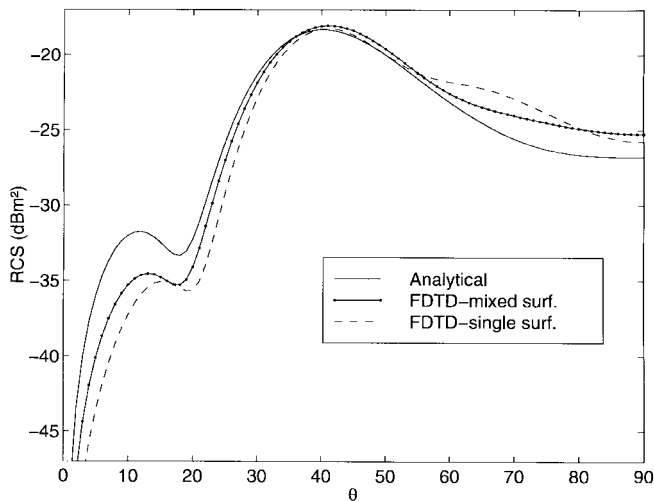
Fig. 11. Bistatic TE-component RCS of circular disk at 2.5 GHz ($\lambda = 12$ cells). Incident field is TE pol. Plane wave is incident from $\theta = 240°$. Scattering angle 0–90° and $\varphi = 90°$.
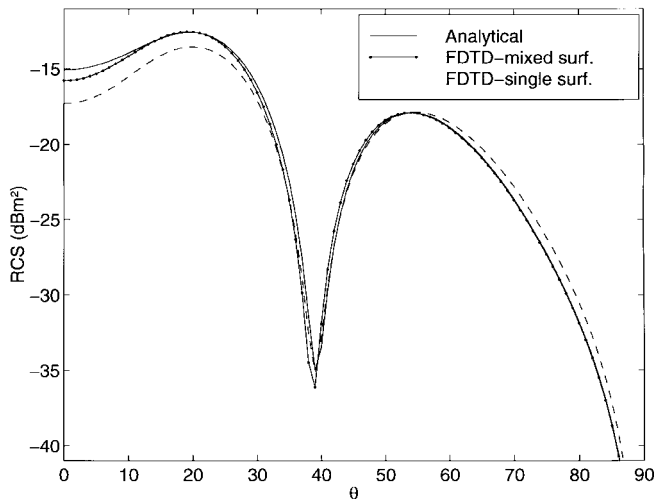

Fig. 12. Bistatic TM-component RCS of circular disk at 2.5 GHz ($\lambda = 12$ cells). Incident field is TE pol. Plane wave is incident from $\theta = 240°$. Scattering angle 0–90° and $\varphi = 90°$.

corresponds better to the analytical result than the single surface transform.

VII. CONCLUSION

It has been shown that by applying the FDTD version of the surface equivalence theorem, the far-zone transformation using vector potentials can be improved. It is important to distinguish between the position of the equivalent current and the position of the field it is calculated from. This transformation procedure not only improves the accuracy, it is also simpler since no spatial interpolation of field values is necessary. Also, the far-zone transformation is further improved by compensating the wavenumber due to dispersion.
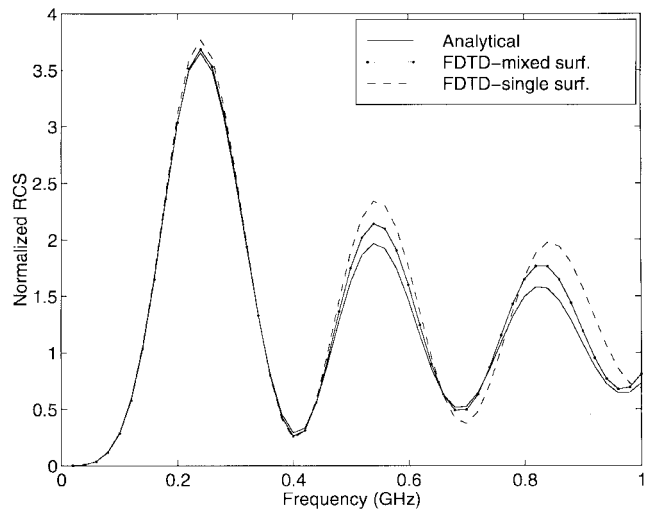
Fig. 13. Normalized monostatic RCS of a sphere as function of frequency. Linear scale.

REFERENCES

[1] K. R. Umashankar and A. Taflove, "A novel method to analyze electromagnetic scattering of complex objects," *IEEE Trans. Electromagn. Compat.,* vol. EMC-24, pp. 397–405, Nov. 1982.
[2] A. Taflove and K. Umashankar, "Radar cross section of general three-dimensional scatterers," *IEEE Trans. Electromagn. Compat.,* vol. EMC-25, pp. 433–440, Nov. 1983.
[3] A. Taflove, K. R. Umashankar, and T. G. Jurgens, "Validation of FD-TD modeling of the radar cross section of three-dimensional structures spanning up to nine wavelengths," *IEEE Trans. Antennas Propagat.,* vol. AP-33, pp. 662–666, June 1985.
[4] R. J. Luebbers, K. S. Kunz, M. Schneider, and F. Hunsberger, "A finite-difference time-domain near zone to far zone transformation," *IEEE Trans. Antennas Propagat.,* vol. 39, pp. 429–433, Apr. 1991.
[5] K. S. Yee, D. Ingham, and K. Shlager, "Time-domain extrapolation to the far field based on {FDTD} calculations," *IEEE Trans. Antennas Propagat.,* vol. 39, pp. 410–413, Mar. 1991.
[6] K. Demarest, Z. Huang, and R. Plumb, "An FDTD near- to far-zone transformation for scatterers buried in stratified grounds," *IEEE Trans. Antennas Propagat.,* vol. 44, pp. 1150–1157, Aug. 1996.
[7] P. B. Wong, G. L. Tyler, J. E. Baron, E. M. Gurrola, and R. A. Simpson, "A three-wave FDTD approach to surface scattering with applications to remote sensing of geophysical surfaces," *IEEE Trans. Antennas Propagat.,* vol. 44, pp. 504–513, Apr. 1996.
[8] O. M. Ramahi, "Near- and far-field calculations in FDTD simulations using Kirchhoff surface integral representation," *IEEE Trans. Antennas Propagat.,* vol. 45, pp. 753–759, May 1997.
[9] D. E. Merewether, R. Fisher, and F. W. Smith, "On implementing a numeric Huygen's source scheme in a finite difference program to illuminate scattering bodies," *IEEE Trans. Nucl. Sci.,* vol. 27, no. 6, pp. 1829–1833, Dec. 1980.
[10] C. L. Britt, "Solution of electromagnetic scattering problems using time-domain techniques," *IEEE Trans. Antennas Propagat.,* vol. 37, pp. 1181–1192, Sept. 1989.
[11] M. J. Barth, R. R. McLeod, and R. W. Ziolkowski, "A near- and far-field projection algorithm for finite-difference time-domain codes," *J. Electromagn. Waves Applicat.,* vol. 6, no. 1, pp. 5–18, 1992.
[12] C. A. Balanis, *Advanced Engineering Electromagnetics.* New York: Wiley, 1989.
[13] J. Fang and D. Xeu, "Numerical errors in the computation of impedances by {FDTD} method and ways to eliminate them," *IEEE Microwave Guided Wave Lett.,* vol. 5, pp. 6–8, Jan. 1995.
[14] A. Taflove, *Computational Electrodynamics: The Finite-Difference Time-Domain Method.* Boston, MA: Artech House, 1995.

[15] J. Svigelj and R. Mittra, "Grid dispersion error using the nonuniform orthogonal finite-difference time-domain method," *Microwave Opt. Technol. Lett.,* vol. 10, no. 4, pp. 199–201, 1995.

[16] G. Kristensson and P. C. Waterman, "The T matrix for acoustic and electromagnetic scattering by circular disks," *J. Acoust. Soc. Amer.,* vol. 72, no. 5, pp. 1612–1625, Nov. 1982.

[17] J.-P. Berenger, "A perfectly matched layer for the absorption of electromagnetic waves," *J. Comput. Phys.,* vol. 114, no. 1, pp. 185–200, 1994.

[18] C. W. Trueman, R. J. Luebbers, S. R. Mishra, and C. Larose, "FDTD computation of the RCS of high permittivity cubes," in *IEEE Antennas Propagat. Soc. Int. Symp.,* Ann Arbor, MI, June 1993, vol. 2, pp. 846–849.

Torleif Martin (S'96) was born in Uppsala, Sweden, on December 27, 1962. He received the M.Sc. degree in engineering physics in 1989 from Uppsala University, Uppsala, Sweden. He is currently working toward the Ph.D. degree in theoretical physics at the Linköping Institute of Technology, Sweden.

From 1989 to 1995, he worked as a System Engineer at Saab Military Aircraft, mainly with electromagnetic environmental effects. Since 1995, he has been working as a Research Officer at the Department of Microwave Technology, Division of Sensor Technology, Swedish Defence Research Establishment. His area of interest includes computational electromagnetics, in particular, the FDTD method.